Mesoscale Conditions for the Severe Convection of 3 April 1974 in the East-Central United States

DENNIS A. MILLER AND FREDERICK SANDERS

Massachusetts Institute of Technology, Cambridge, Mass 02319

(Manuscript received 6 November 1979, in final form 14 January 1980)

ABSTRACT

Hourly surface observations from more than 200 stations, together with routine radar and rawinsonde data, are used to elucidate the mesoscale conditions for the extraordinarily widespread severe convection in the central United States on 3 April 1974. Strong mesoscale pressure fluctuations on an hourly time scale, particularly intense north of the Ohio River, were superposed on a substantial synoptic-scale pressure fall associated with the northeastward advance of a deep cyclone toward the Great Lakes. Most of this mesoscale variation was associated with 10 wavepackets of considerable spatial and temporal continuity. The character of the accompanying wind and weather fluctuations was highly suggestive of gravity-wave activity. The packets were aligned approximately along the low-level wind flow and propagated to its right at speeds of ~30 kt.

Three major regions of organized convection were present, also oriented approximately parallel to the low-level flow and separated by ~150 n mi. These regions propagated to the right of this flow at speeds of ~20 kt and appeared to arise from a source other than the presumed gravity waves. Rather, the convection appeared to initiate the waves, in at least some instances. More generally, the overtaking of a slow-moving convective region by a rapidly moving wave caused an increase in intensity of convection, a reformation of a line of radar echoes within the region, and an increase in the pressure amplitude of the wave.

1. Introduction

The tornado outbreak of 3–4 April 1974, in the central and southern United States, was the worst in recorded history. Fujita (1975) identified 148 tornadoes, many extremely destructive, in 13 states during the 12 h period beginning at 1800 GMT on the 3rd. Fig. 1 shows the damage paths of these storms.

Hoxit and Chappell (1975a) have presented a comprehensive analysis of the synoptic-scale aspects of this case, finding that the tornadoes occurred in a region where ascent associated with an intense cyclonic system acted on an unusually large volume of potentially unstable tropical air. Recognition of these circumstances at the time, in fact, had led to a remarkably skillful delineation of the general area of the severe convection by the National Severe Storms Forecast Center (NSSFC) several hours before the onset of the activity, as seen in Fig. 1.

On the other hand, much disagreement exists concerning the mesoscale mechanisms of organization of severe convection in space and time. Substantial advance in the precision with which this activity can be skillfully predicted awaits the achievement of a useful understanding of these mechanisms. Relevant theories are not developed to the point where they can be unambiguously tested against observations; but neither are many observations analyzed so that tests can be made, since the mesoscale structures are subliminal with respect to the routine synoptic network. In this paper we wish to describe the mesoscale environment in which the severe storms developed in this case, principally through study of radar data and of routine surface observations.

2. Synoptic conditions

The synoptic conditions for the major tornado outbreak are illustrated in Fig. 2. A major cyclonic disturbance, strongly developed through the entire depth of the troposphere, moved northeastward across the central plains at a moderate speed toward the Great Lakes. Warm advection in the lower troposphere together with strong cyclonic vorticity advection in the upper troposphere implied substantial ascent over much of the eastern half of the United States, from the low-pressure trough eastward to the Appalachians. The conventional frontal structure as such was not especially marked and played little role in the development of convection, although overall synoptic-scale temperature contrasts were substantial. Of particular interest is the large area of strongly negative lifted index (Galway, 1956), indicating the convective potential of the warm

0022-4928/80/051041-15$07.75

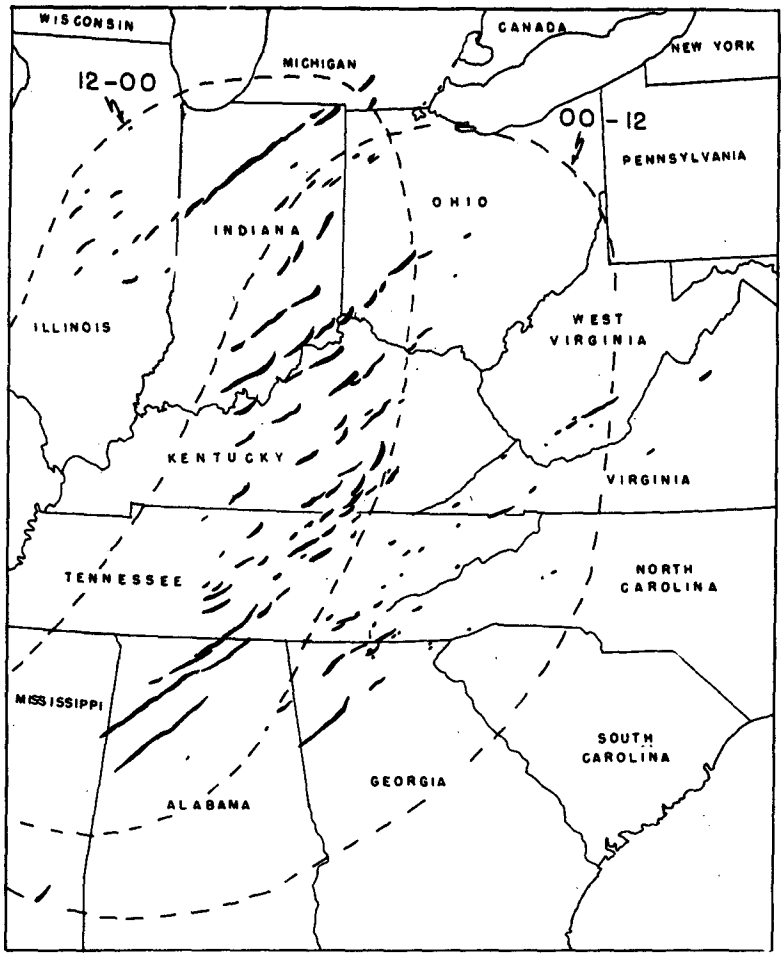

FIG. 1. Tornado damage tracks, 3–4 April 1974, after Fujita (1975). Dashed lines show area of severe thunderstorms predicted by NSSFC for the 12 h periods beginning 1200 GMT 3 April and 0000 GMT 4 April.

moist tropical air entering the system from the Gulf of Mexico.

3. Data sources for the mesoscale analysis

The major source was a set of copies of the observer's forms for the 3 April (local time) hourly and intermediate (special) surface observations at more than 200 stations in and around the region of severe convection. The convective activity was studied by examination of the subjectively prepared radar summary charts produced hourly by NSSFC. Conventional synoptic rawinsonde observations completed the inventory of available information. A map showing the location of surface observations, upper level soundings and radar observations appears as Fig. 3.

4. Analysis of the time series of surface observations

Time series of observations of altimeter setting (station pressure reduced to sea level on the basis of standard atmospheric temperature profile) are shown in Fig. 4, together with meteorological and other events, for three stations. These represent conditions in the northern, central and southern portions of the region of severe convection. The sequence of hourly data shows a lengthy period of pressure fall ending around 2300 GMT, due to the approach of the cyclone. Hour-to-hour variability is also evident, implying the presence of mesoscale troughs and ridges. The additional special observations suggest that the features shown by the hourly data alone are not crucially aliassed by the presence of shorter period variations. (Fortunately, the tornado cyclone at SDF fell between the 2100 and 2200 GMT observations.)

To establish temporal and one-dimensional spatial continuity, we analyzed a dozen time sections which either passed through stations or to which station positions were projected. The lines appear in Fig. 3, and an example is shown in Fig. 5. It is immediately clear that many, though not all, substantial meso-

scale falls and rises had considerable continuity. The more prominent of these, identified as explained later, were assigned letters, which also appear in Fig. 4.

Thunder, hail and rain tended to occur on rising pressure or on the mesoscale ridge between rising and subsequently falling pressure, as typically found in studies of intense convective storms. The

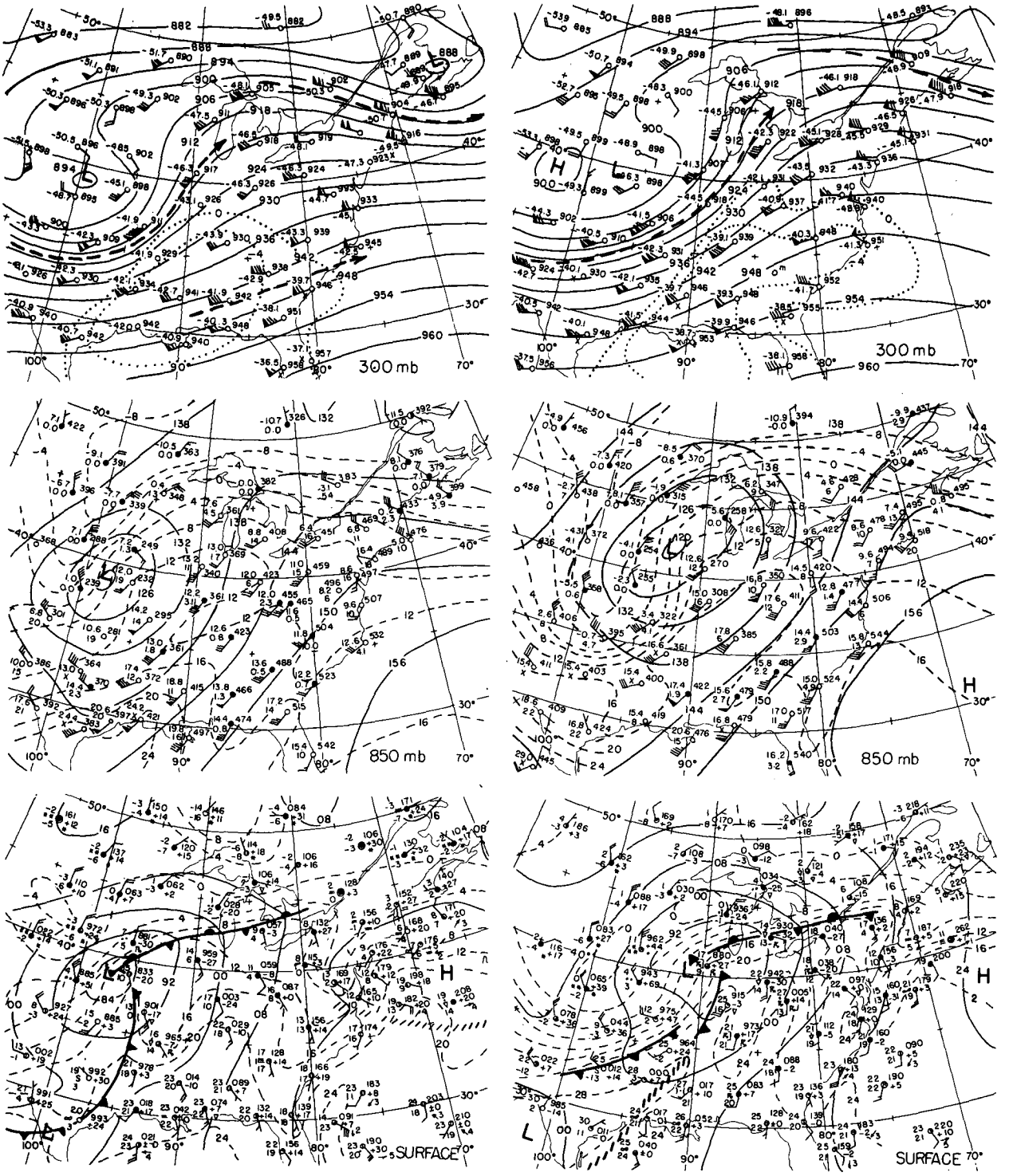

FIG. 2. Synoptic-scale analyses for 1200 GMT 3 April (left column) and for 0000 GMT 4 April (right column). Solid lines on surface charts are sea level isobars at 8 intervals; on the 850 and 300 mb charts they are MSL height contours at 6 dam intervals. Thin dashed lines are isotherms at intervals of 4°C. On 300 mb charts heavy solid arrows represent positions of jet streams and dotted lines are 0°C and −4°C isopleths of lifted index. Plotting models are conventional.

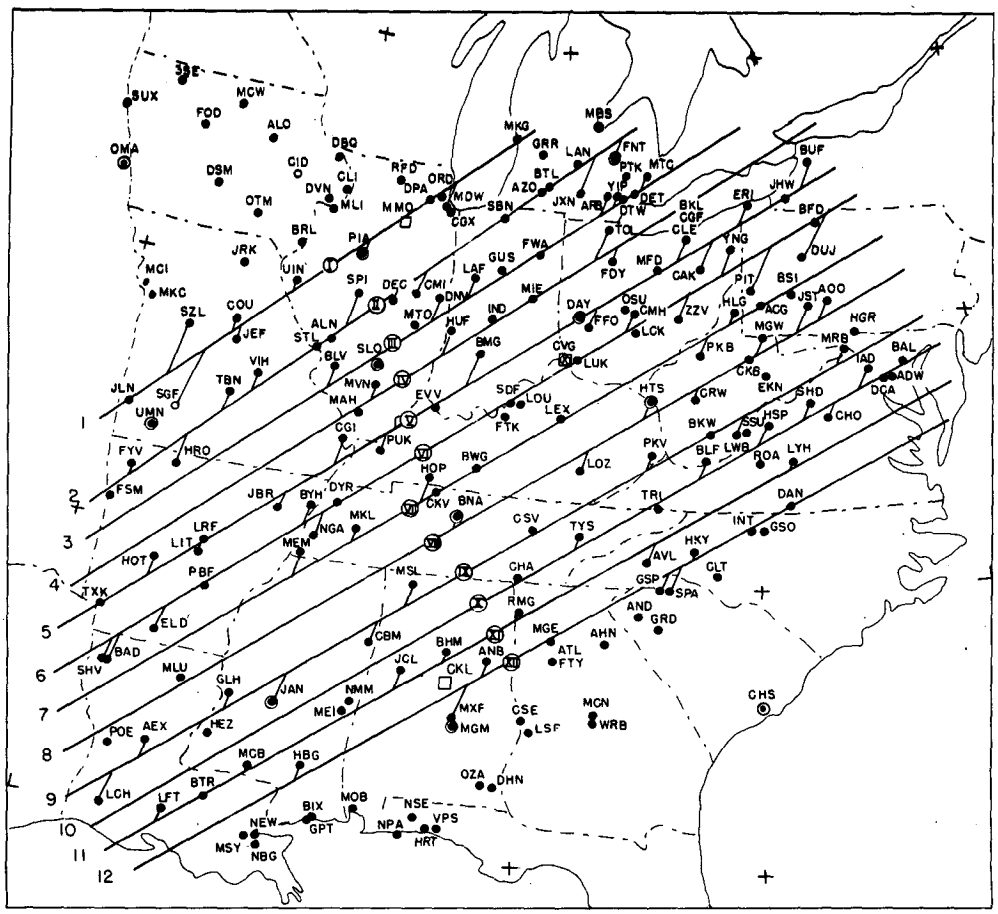

FIG. 3. Locations of stations, identified by three-letter call signs. Circled dots indicate rawinsonde locations. Squares show radar sites. Time-section lines are indicated.

wind tended to back slightly at the mesoscale trough between fall and subsequent rise and to veer at the ridge. While some cooling occurred with the onset of precipitation the strong veering winds and abrupt drops in temperature characteristic of a thunderstorm gust front were seen only between VIH and CMI from 1700 and 2100 GMT. The pressure perturbations here were modest, although a tornado was embedded in the mesoscale trough at DEC. The activity on the whole in this section was suggestive of gravity waves.

5. Mesoscale pressure activity and vertical temperature structure

The time-section analyses indicated that the hourly-scale pressure activity was more marked in the north than elsewhere. As a measure of the mesoscale intensity of an hourly change, the magnitude of the difference between its value and the average of the values for the two immediately adjacent hours was taken. For example, in Fig. 4 the rise at FWA from 1500 to 1600 GMT was 0.05 inch. The average for the preceding and following hours was a fall of 0.055 inch, yielding an intensity of 0.105 inch (proportional to the magnitude of the second local time derivative of pressure). On this basis, at each station a count was made of the number of instances in which the isallobaric intensity exceeded 0.06 inch, with results mapped in Fig. 6.

This figure shows that intense mesoscale pressure activity was widespread roughly north of the Ohio River. The surface analyses (Fig. 2) show relatively cool air in this region, although no synoptic-scale front was evident. An average temperature profile from 975 to 525 mb for soundings north of the river at 1200 GMT 3 April is contrasted in Fig. 7 with a corresponding average at stations in the general region of future convection to the south. A similar comparison of mean soundings at 0000 GMT 4 April is also shown in Fig. 7. The main difference in the profiles is the markedly stable air in the lowest 50 mb at the northern stations. In the south the surface boundary layer was only slightly stable at 1200 GMT

and was nearly adiabatic at 0000 GMT. Above the boundary layer, the deep conditional instability was interrupted in the south by slightly stable layers reflecting sharp shallow inversions at individual stations.

It is clear that frequent large-amplitude hourly-scale pressure fluctuations occurred preferentially in a temperature structure in which cool stable air near the ground was capped by conditionally unstable air. Examination of hourly observations at southern stations showed that the few intense mesoscale pressure events occurred almost without exception in rain-cooled air at the surface, with a presumed local temperature structure similar to that shown at the northern stations. This structure agrees qualitatively, with that proposed by Lindzen and Tung (1976), although a 50 mb depth of the wave duct yields much too slow a propagation speed.

6. Horizontal mapping of the wave packets

To obtain a satisfactory view of the mesoscale pressure activity, we must consider the two-dimensional, horizontal picture rather than the single spatial dimension in the time sections. Accordingly, we defined a wavepacket in the station record as starting with an hourly fall separating a trough from the following rise and ending on a ridge. The falls and rises may be only relative to the neighboring values. The strength of the packet was considered to be the sum of the strengths of the hourly fall and of the hourly rise, defined as in the preceding section. Packet strengths of at least 0.09 inch were considered strong, those between 0.06 and 0.09 inch moderate, and others weak. To obtain perspective, consider that an otherwise steady series of pressure values perturbed downward by 0.01 inch one hour and upward 0.01 inch the next would yield an intensity of 0.05 inch.

The times of all strong events were mapped for all stations. Likewise, maps of the times of moderate and weak events were prepared. Then events were sorted into groups which were characterized by reasonable spatial and temporal continuity. It was not necessary to assume explicitly a more or less meridional orientation and an eastward progression. Rather, these characteristics seemed to be unavoidable. This important and subjective analysis was done independently by the senior author and by Professor L. F. Bosart, both of whom were careful to be unaware of the details of the convective activity until after completion of the analyses. The two sets of analyses were in close agreement except in western Illinois around 1600 GMT and in the Appalachian Mountains, in general, where packets tended to lose coherence. The identified set of packets incorporated ~90% of the strong and moderate events.

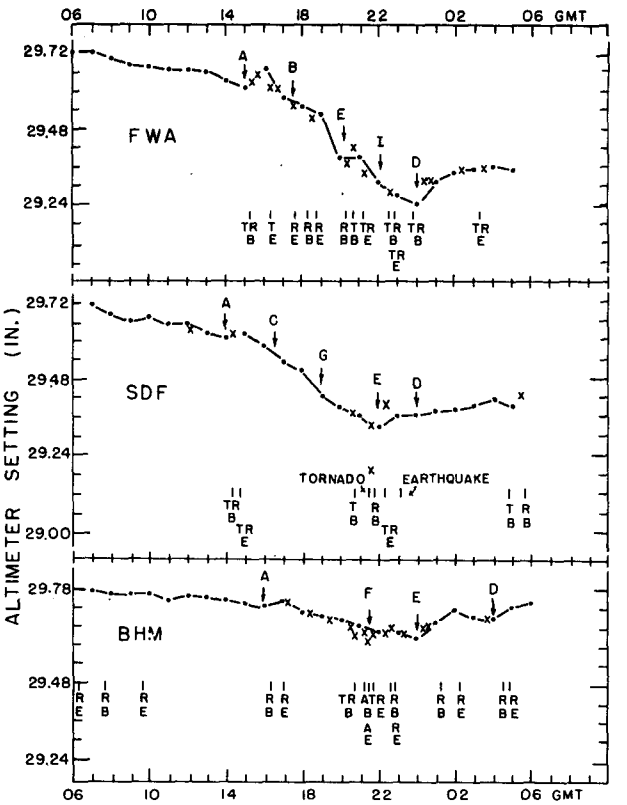

FIG. 4. Time series of surface observations, 3–4 April. Dots connected by straight line segments are regular hourly observations of altimeter setting. Additional intermediate observations are shown by ×'s. Tick marks indicate times of beginning (B) or ending (E) of rain (R), thunder (T) and hail (A). Other events of geophysical interest are spelled out. Letters with arrows denote the times of passage of analyzed mesoscale troughs.

Isochrones for 10 packet troughs, as determined by the senior author, are shown in Fig. 8. They are designated by letters, assigned chronologically according to the time of initial appearance, a number of which appear in Figs. 4 and 5. The speed of progression of the packets can be compared with vector mean winds for the layers from the surface to 750 mb, from 750 to 500 mb and from 500 to 250 mb, as shown in Fig. 8. The sounding nearest in time to the time of local passage of each packet was selected.

It is clear from Fig. 8 that in virtually all instances the packets are oriented approximately parallel to the lower tropospheric flow and are propagating to the right of it, at relative speeds as high as 50 kt. It is also clear that in most instances the packet propagation speed is matched by the normal component of the mean wind in the middle or upper troposphere, in agreement with Lindzen and Tung's (1976) prescription for strong reflection of gravity waves propagating vertically from below.

The behavior of the surface wind as the identified

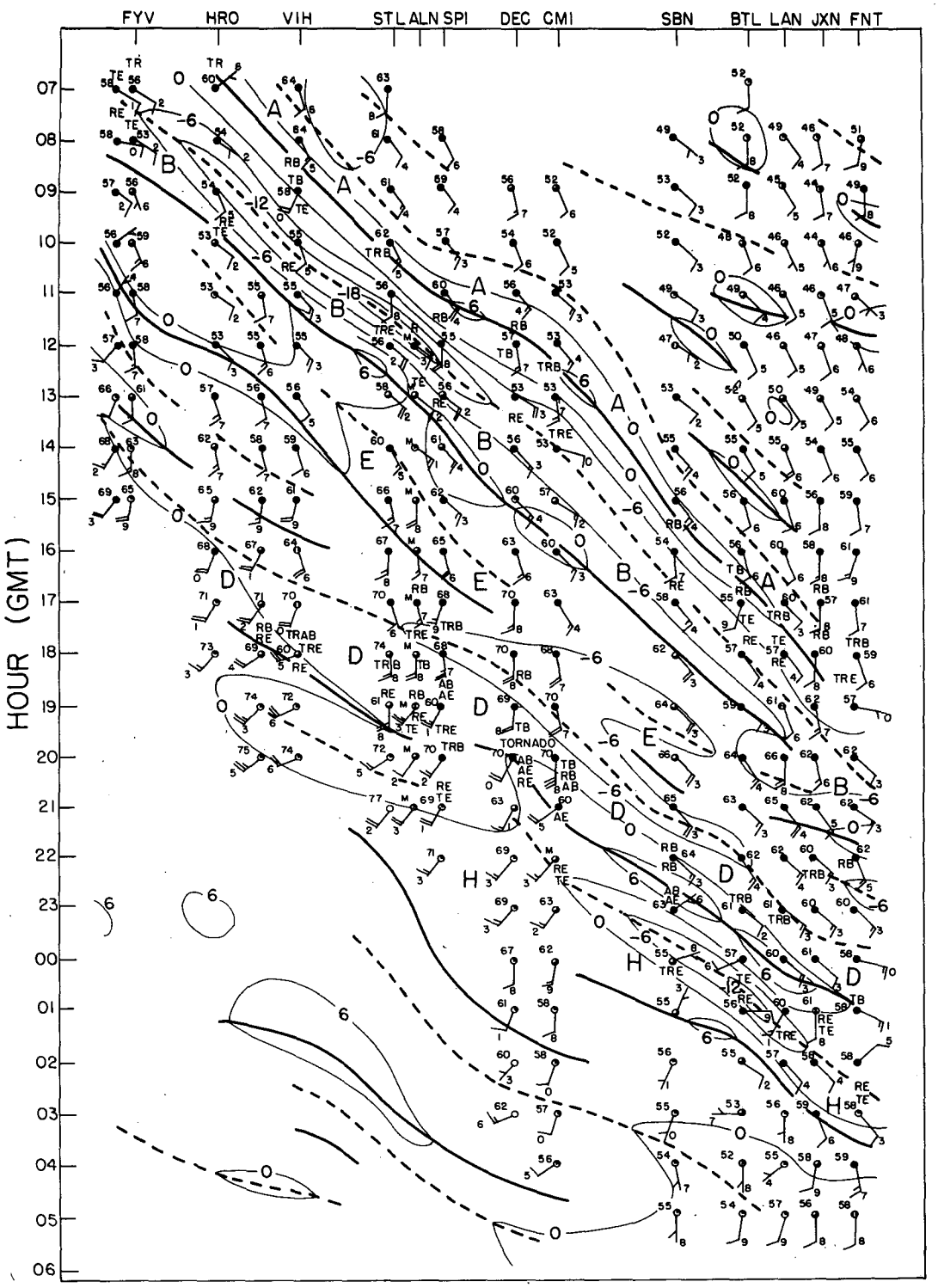

FIG. 5. Time-section II (see Fig. 3). Thin lines are isopleths of hourly change of altimeter setting, labelled in hundredths of inches. Plotting model is conventional, except that tens of degrees digit for wind direction is shown next to wind barbs. Surface temperatures are in °F and north is considered at the top of the diagram for the purpose of wind plotting. Times of events of interest, denoted as in Fig. 4, are shown. Heavy dashed and solid lines represent local minima and maxima, respectively, of 1 h change in altimeter setting. Large letters show approximate positions of analyzed troughs.

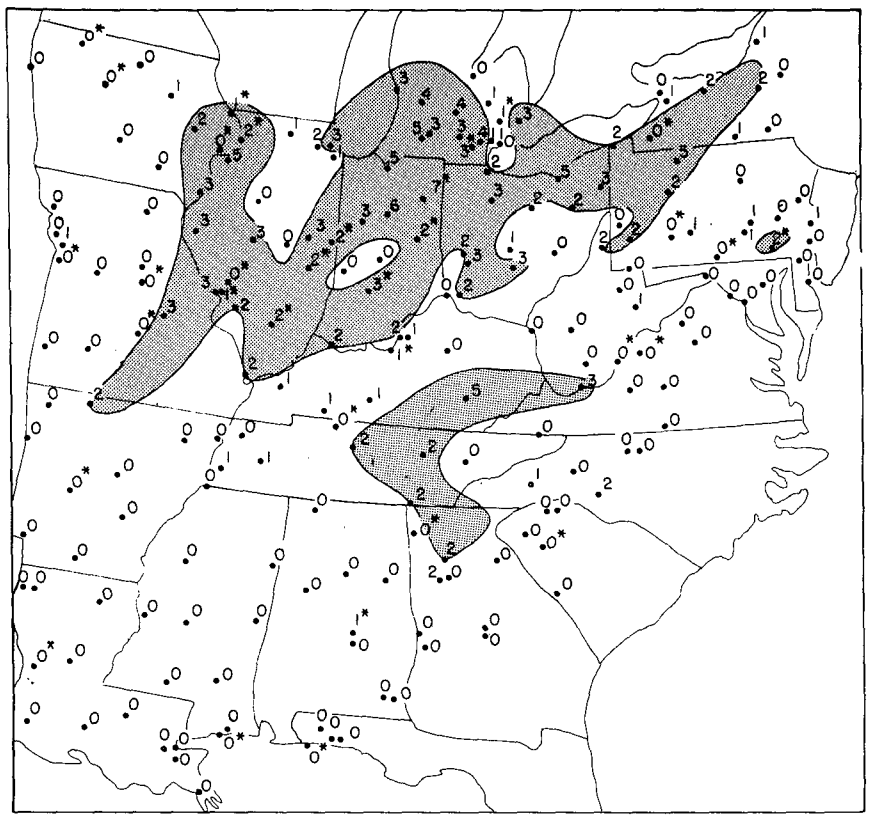

FIG. 6. Map of number of instances of large 1 h mesoscale pressure tendencies on 3 April (LST). See text for definition. An asterisk indicates an incomplete station record. The stippled area indicates two or more instances.

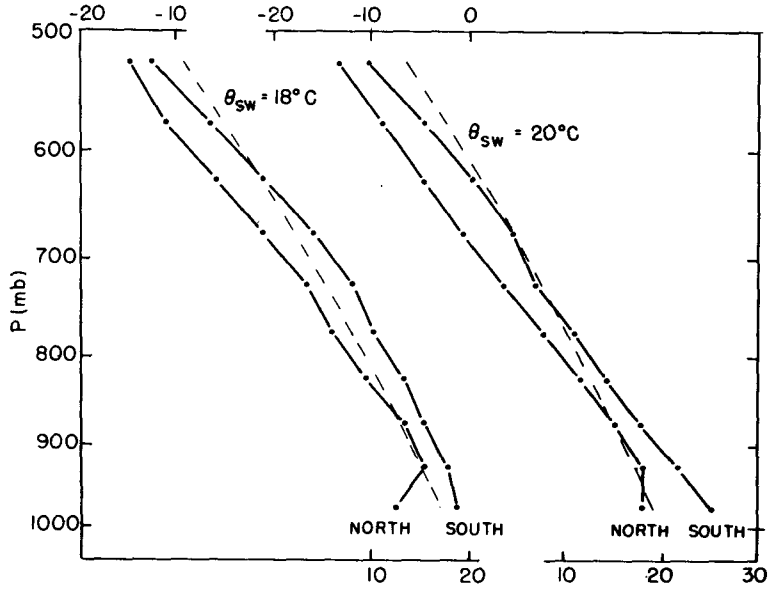

FIG. 7. Mean temperature soundings with a moist adiabat for reference, from stations in the convective areas north and south of the Ohio River. The sounding pair for 1200 GMT 3 April is to the left; the pair for 12 h later is to the right.

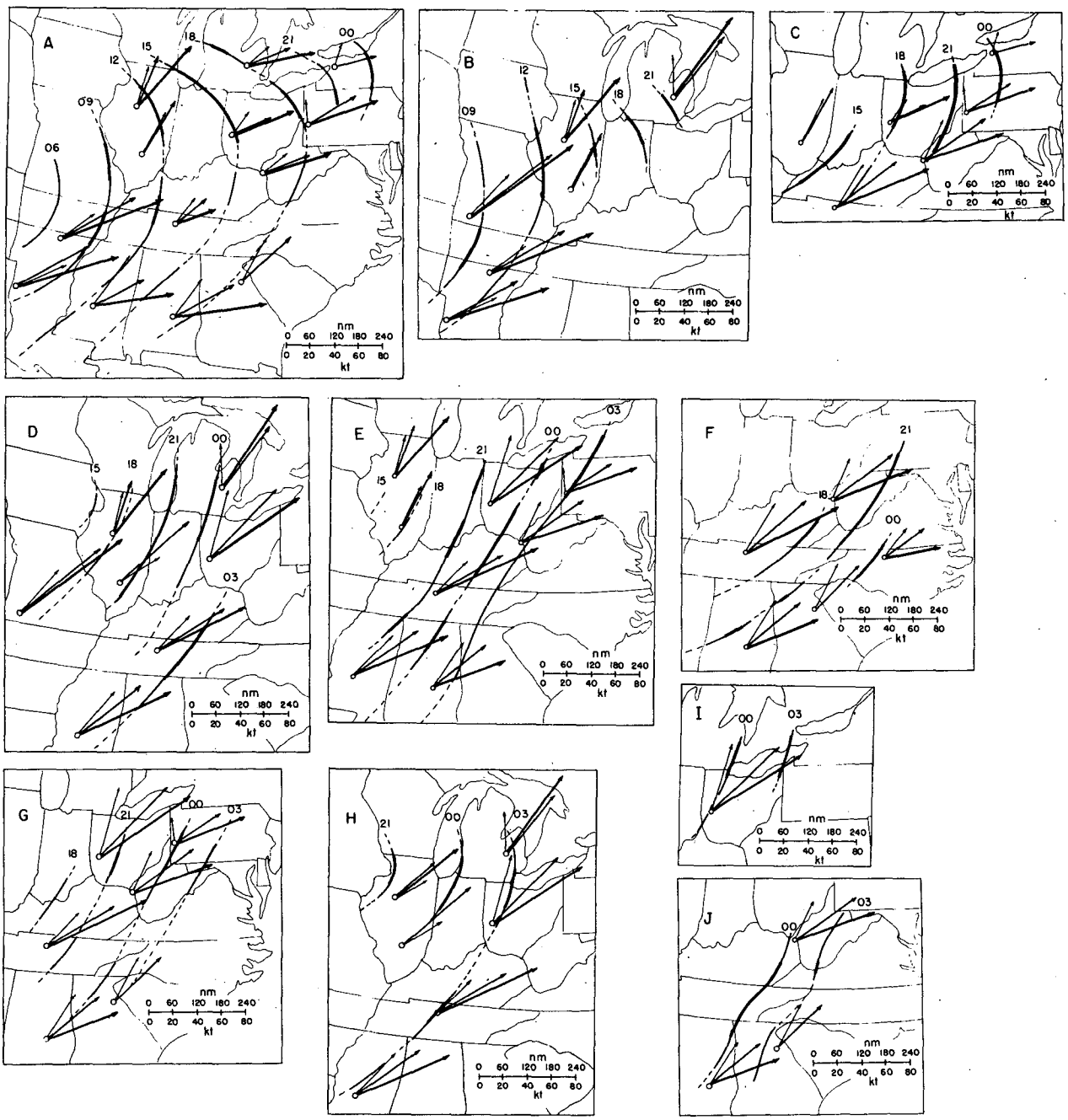

FIG. 8. Three-hour isochrones of troughs of analyzed wavepackets A–J, with GMT labels. Thick, thin and dashed portions show large, moderate and small packet strength, as explained in the text. Light, medium and heavy arrows represent mean winds in the lower, middle and upper troposphere, with length equal to a 3 h displacement at the appropriate speed.

packets passed the stations contained in Sections 2, 5 and 9 is summarized in Table 1. At each station the time of trough or ridge passage was taken to be whichever of the two nearest hours yielded a result more favorable to our preconception. This prejudice, confirmed by the results, is that the wind backs prior to trough passage, veers until ridge passage and then backs. This behavior is consistent with the interpretation of the changes as due to gravity wavepackets.

A study of surface wind speeds during packet passage revealed little systematic variation on the average over all packets appearing on the three sections. The mean speed varied no more than 1 kt over the hourly categories shown in Table 1. The hourly observation showing the highest peak gust occurred

TABLE 1. Changes of wind direction (deg) during the hours before and after the passage of the trough and before and after the ridge, for wavepackets present on time sections II, VI and IX.

Packet	N	Before trough		After trough		Before ridge		After ridge	
		Mean	SD	Mean	SD	Mean	SD	Mean	SD
A	33	−7	±14	+22	±19	+25	±19	−32	±29
B	19	−15	±30	+13	±16	+16	±13	−3	±20
C	13	−10	±16	+15	±27	+15	±27	−14	±28
D	13	±0	±17	+48	±38	+42	±49	−32	±50
E	21	+6	±44	+12	±24	+15	±18	−5	±16
F	5	−10	±10	+14	±11	+14	±21	−16	±15
G	9	−9	±20	+53	±60	+54	±59	+3	±64
H	8	−42	±61	+26	±43	+42	±59	−49	±62

about twice as frequently at the hours of falling pressure preceding the trough and following the ridge as at hours during trough and ridge passage and in between. There is thus some indirect evidence of vorticity in the boundary layer above the standard 10 m level of surface wind observations: cyclonic near the trough and anticyclonic near the ridge. Strong peak gusts associated with thunderstorms tended to occur between trough and ridge but rarely affected the regular hourly observations.

The occurrence of precipitation was studied in relation to packet passage at stations on all 12 time sections. At each station the mid-time of each precipitation episode shorter than 3 h duration was determined. This time was then associated with either the fall, the trough, the rise or the ridge. Frequencies of these categories, and of the categories of none and of continuous precipitation (3 h duration or more), are given in Table 2 for each wavepacket.

Note from the results that no precipitation accompanied the packet in almost half the instances and that about three-fourths of the precipitation episodes occurred with rising pressure or near the mesoscale ridge. This relationship is consistent with the mesoscale pattern of vertical motions accompanying gravity waves, as pointed out also by Uccellini (1975).

The packets displayed a number of individual characteristics: A showed a remarkable concentration of precipitation episodes at the pressure ridge; E, F and I showed episodes relatively evenly distributed throughout the mesoscale pattern; B and C were associated with relatively little precipitation. These characteristics will be clarified when we have examined the pattern of convection as shown by the hourly radar summary charts.

7. Convection as observed by radar

Manually prepared radar summary charts were examined for the period from 2335 GMT 2 April to 0535 GMT 4 April. The great mass of information, representing subjective interpretation for the most part, was difficult to analyze. We decided to deal with individual cells, denoted on these charts because of their great height, either absolutely or in relation to their neighbors. We felt that the most intense aspects of the convection was thus captured with a maximum of objectivity. Positions of cells for successive groups of 5 h are plotted in Fig. 9, for the

TABLE 2. Frequency of occurrence of precipitation episodes by category of mesoscale pressure pattern. Values in parentheses are percentage frequencies.

Wave-packet	Falling pressure	Near trough	Rising pressure	Near ridge	Continuous precipitation	No precipitation	N
A	1 (01)	1 (01)	13 (13)	53 (54)	0 (0)	30 (31)	98 (100)
B	1 (02)	2 (04)	3 (07)	4 (09)	0 (0)	35 (78)	45 (100)
C	0 (00)	3 (08)	1 (03)	5 (14)	0 (0)	27 (75)	36 (100)
D	1 (02)	3 (07)	20 (44)	9 (20)	3 (07)	9 (20)	45 (100)
E	6 (10)	5 (9)	10 (17)	8 (14)	2 (03)	27 (47)	58 (100)
F	3 (09)	3 (09)	4 (13)	5 (16)	1 (03)	16 (50)	32 (100)
G	3 (09)	4 (12)	12 (36)	7 (21)	0 (0)	7 (21)	33 (100)
H	1 (03)	1 (03)	6 (17)	7 (19)	0 (0)	21 (58)	36 (100)
I	1 (06)	2 (13)	4 (25)	1 (06)	2 (13)	6 (38)	16 (100)
J	0 (00)	2 (22)	1 (11)	3 (32)	2 (22)	1 (11)	9 (100)
All	17 (04)	26 (06)	74 (18)	102 (25)	10 (02)	179 (44)	408 (100)

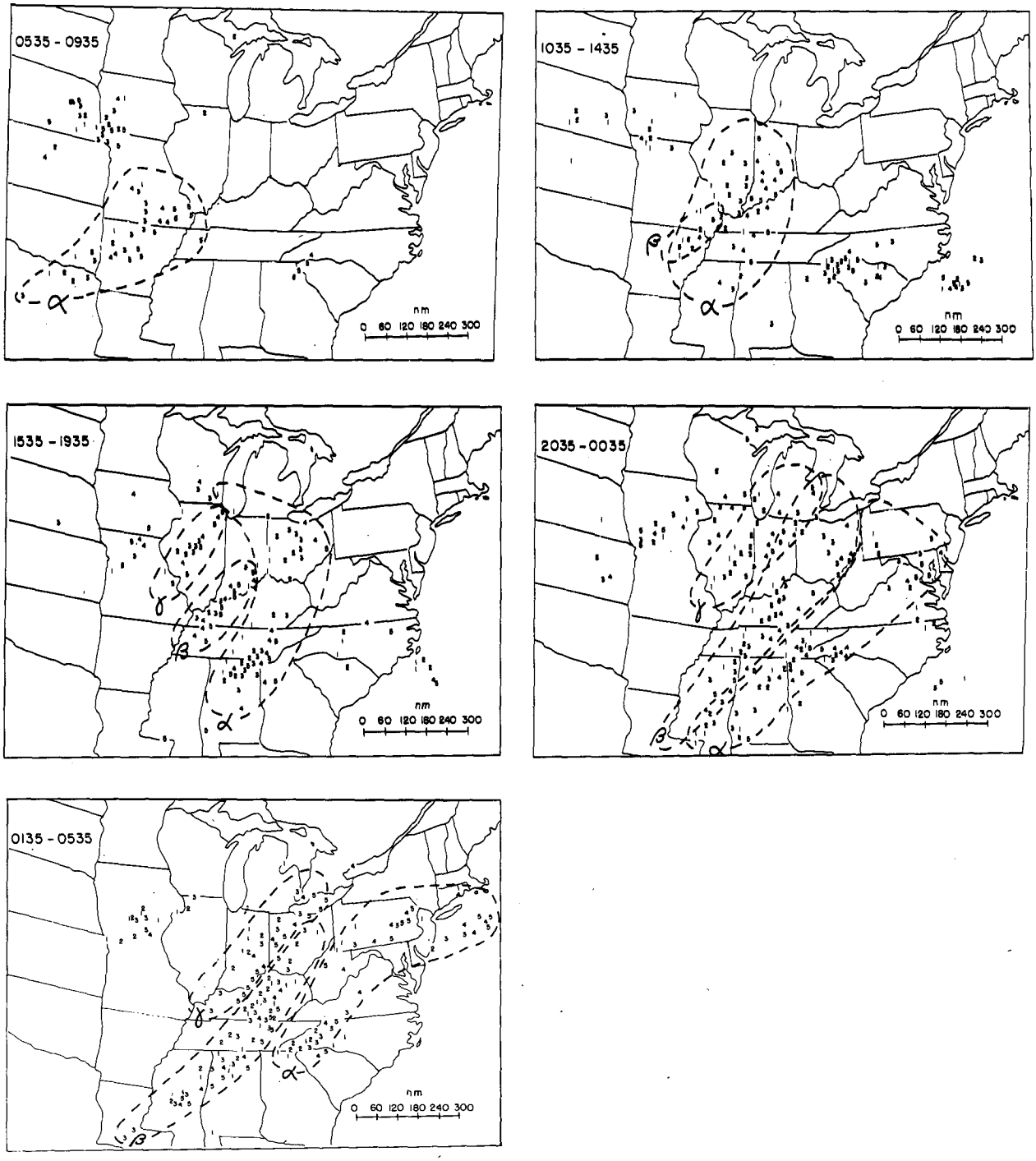

FIG. 9. Convective cells as shown in the hourly radar summary charts for each consecutive group of 5 h from 0530 GMT 3 April to 0535 GMT 4 April. Digits indicate the sequence of hours within each group. Dashed lines enclose the cells associated with convective areas α, β and γ.

period starting 0535 GMT 3 April, the approximate time of beginning of our surface mesoanalysis.

In the first group, from 0535 to 0935 GMT, we see a moving group of cells centered in Arkansas, denoted convective area α, and another scattering of cells with less coherent movement north and northeast of the surface cyclone center in Kansas (cf. Fig. 2). None of the latter group produced severe thunderstorms.

The next group of hours shows rapid northeastward motion of area α, the centroid moving at ~50 kt. It further shows at 1235 GMT the initial develop-

ment of a new region of convection in northeastern Arkansas. This new area β lay ~180 n mi northwest of the concurrent position of area α.

The hours from 1535 to 1935 GMT show continuing eastward displacement of most of area α. Close inspection shows that the retardation of its southern portion was due to the development of new cells, starting at 1835 GMT, ~90 n mi northwest of the easternmost cells. Area β extended substantially northeastward but the elongated area propagated southeastward at only ~15 kt.

A third region of subsequent severe convection, area γ, developed from eastern Missouri to northeastern Illinois. Its southeastward propagation speed was also ~15 kt. Areas α (except for its northernmost position), β and γ were all elongated parallel to the lower tropospheric flow (cf. Fig. 8) with a nearly uniform spacing of ~150 n mi. In fact an additional large single storm complex is seen to have moved north-northeastward from western Missouri to southeastern Iowa, its track lying another 150 n mi northwest of area γ.

This orderly arrangement of the new convection beginning on 3 April seems unlikely to have been a coincidence. Darkow and Livingston (1975) suggest that our area γ may have originated from a northward extension of surface air with high moist static energy along the Mississippi River, but their maps do not show overall organization on the same scale as the convection.

During the period from 2035 to 0035 GMT no new regions appeared. Areas α and β developed southwestward to the Gulf Coast. The southern portion of all three areas propagated southeastward at ~15 kt. The northern portion of α continued to advance eastward at near 50 kt. Northern portions of areas β and γ moved eastward at ~25 kt.

At 2335 GMT we see within area β the first signs of development of new cells in Kentucky ~70 n mi northwest of the original line. Forbes (1975) has suggested that the resulting double line is a consequence of relative motion of rotating and nonrotating thunderstorms. His data, however, show a difference of only 6 kt along the line-propagation direction of 120°, too slow to account for the observed separation in the limited time available. We favor an alternative explanation, to be advanced later.

A group of cells in eastern Ohio within area β between 2235 and 0035 GMT appeared to be a separate development, but the effect was probably spurious since the purportedly cell-free region in southwestern Ohio was struck by several tornadic thunderstorms at this time. Temporary failure of the radar at CVG was probably responsible for the gap in data presented in the summaries.

The hours between 0135 and 0535 GMT 4 April showed the dissipation of much of area α (or possibly its motion out of radar range in the central Appalachian Mountains where a number of tornadoes occurred at this time). Within area β the northwestern line became the important one of the pair and advanced southeastward at ~25 kt. Area γ likewise moved southeastward at ~25 kt.

Overall, the convective areas, except for the northern portions of α, moved southeastward more slowly than the pressure wavepackets (say, 23, 17 and 16 kt for α, β and γ, respectively) and ~30 kt for the packets (cf. Fig. 8). A similar difference was noted by Uccellini (1975). Next we examine resulting interactions between the two.

8. Interactions between the wavepackets and the convection

A series of maps at 3 h intervals shows in Fig. 10 the relative positions of the packet troughs, the convective areas, and the cells and lines shown on the radar summaries, from 0535 GMT 3 April to 0235 GMT 4 April. Packets A and B entered the region of the analysis by 0835 GMT, closely associated with convection evidently organized farther west during the preceding day.

Packet A led its band of convection (area α) across the entire region of study, the portion south of Pennsylvania dissipating after 1735 GMT. (Bosart's analysis shows a southward extension of A corresponding to the convection in Delaware at 2335 GMT, and is preferred.) No tornadoes or excessive winds occurred but hail fell in southwestern Ohio around 1600 GMT from relatively modest cells. No other packet had such a simple and long-lasting relationship to a convective line. The structure appears to be an example of wave-CISK, as suggested by Lindzen (1974) and Raymond (1975).

Packet B was a sort of wake depression following A. It persisted long after 1135 GMT only in the northern part of the area of analysis and was hydrometeorologically and convectively innocuous (cf. Table 2) although displaying considerable strength in the pressure field.

Packet C appeared as a wake depression around 1435 GMT, replacing part of the dissipated packet B. It also was associated with little precipitation despite its origin close to some cells in the western portion of area α.

Packet D appeared in eastern Iowa around 1435 GMT in a region of broken but generally unremarkable radar echoes. It progressed across northwestern Illinois at 1735 GMT as a weakened and marginally detectable feature. By 2035 GMT, packet D had overtaken convective region γ. In this interaction the packet grew greatly in intensity (cf. Fig. 8) and the line became tornadic as seen in Table 3. This spate of tornadoes across Illinois and northern Indiana has been studied in relation to the meso-

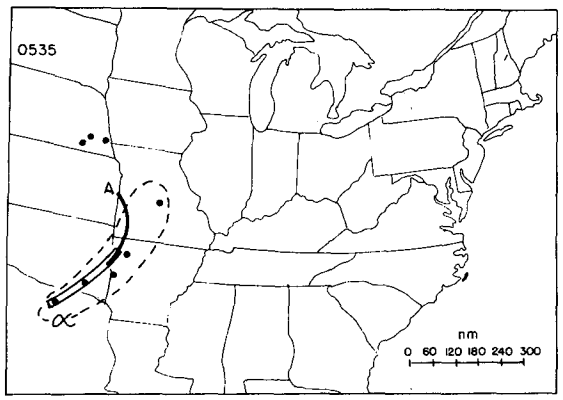
0535
A
α
nm
0 60 120 180 240 300

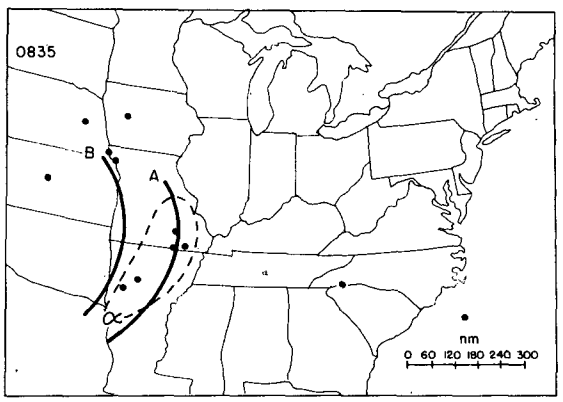
0835
B
A
α
nm
0 60 120 180 240 300

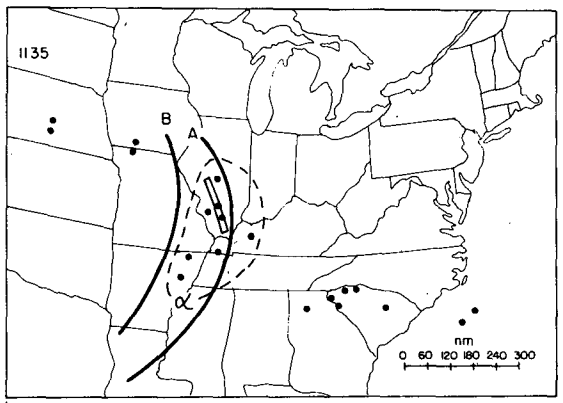
1135
B
A
α
nm
0 60 120 180 240 300

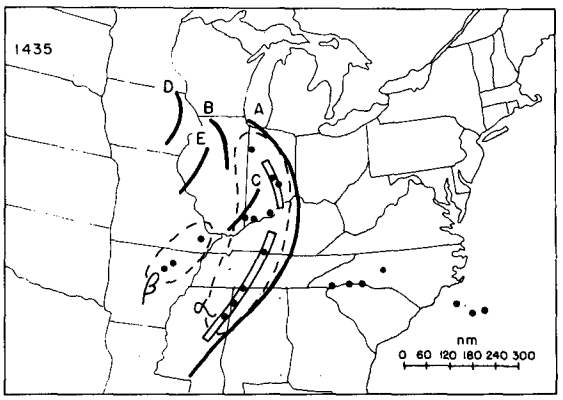
1435
D
B
A
E
C
β
α
nm
0 60 120 180 240 300

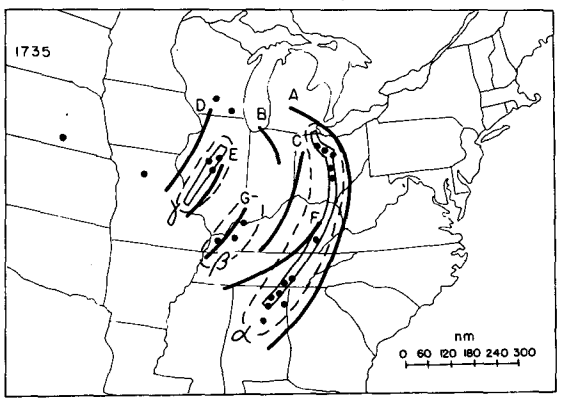
1735
D
B
A
C
E
G
F
β
α
nm
0 60 120 180 240 300

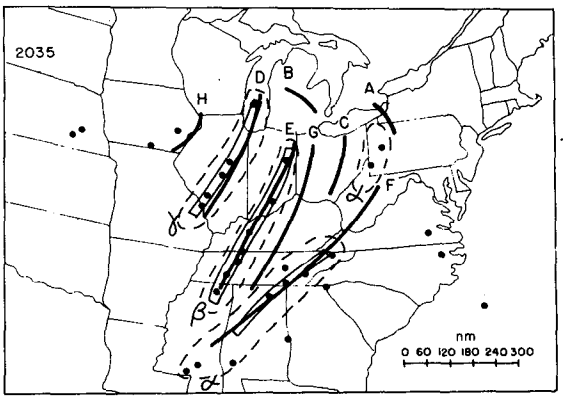
2035
H
D
B
A
E
G
C
F
α
β
nm
0 60 120 180 240 300

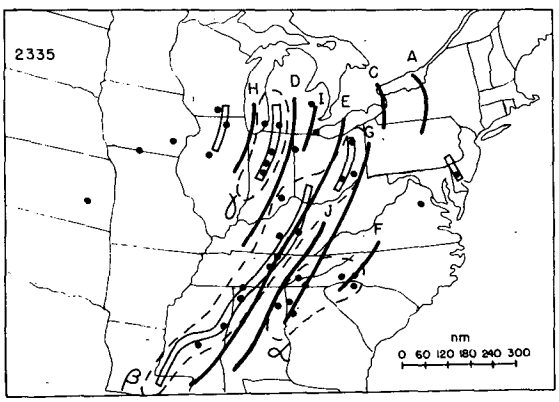
2335
H
D
I
E
C
A
G
F
α
β
nm
0 60 120 180 240 300

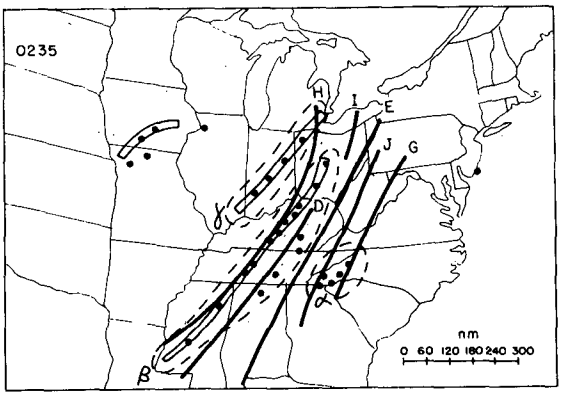
0235
H
I
E
J
G
D
α
β
nm
0 60 120 180 240 300

scale pressure pattern by Hoxit *et al.* (1976) and Forbes (1975). In this instance the relationship was close but it should be borne in mind that numerous equally destructive tornadoes occurred on this day south of the Ohio River with very little hourly-scale pressure activity.

Packet D had not finished. Between 2335 and 0235 GMT it grew rapidly southward, overtaking area β, which had already produced numerous destructive thunderstorms. The clearest interaction appeared to be the formation of the northwestern line of cells discussed earlier, as the overtaking occurred. Production of tornadoes in area β was a maximum between 2300 and 0100 GMT, but they were almost equally numerous from 2030 to 0230 GMT, as indicated by the data in Table 3.

Packet E first appeared, weakly, in western Illinois at about 1500 GMT. An hour and a half later the first echo appeared on the radar summary at 1635 GMT. Another hour later a substantial line (area γ) was present in central Illinois. Since the convection must have started before the first echo appeared it is difficult to say whether area γ or packet E came first. It was essentially simultaneous.

Packet E immediately moved away from area γ and overtook area β at 2035 GMT. As in the interaction between D and γ, the result was a considerable strengthening of the packet. Area β was already tornadic but the considerable increase in numbers of tornadoes shortly after 2030 GMT may be attributable to the overtaking. The line in area β moved briskly eastward with packet E the next 3 h, after which both weakened.

Packet F appeared around 1735 GMT, like C a depression in the wake of packet A, largely in a precipitation-free region. In the following 3 h, however, it interacted with convective area α, now left behind by the dissipating packet A. New cells developed to the west of the original line at 1835 GMT, as mentioned earlier. By 2035 GMT a coherent line coincided with packet F and the first two of numerous tornadoes produced by area α had occurred as seen in Table 3. The more numerous later tornadoes in this region, however, could not be unambiguously related to the wavepackets. Nor did the convection in area α appear to be very well organized.

Packet G appeared in western Kentucky at about 1700 GMT in a group of rapidly growing and proliferating cells (area β). As with E and γ, packet G moved away from area β as the latter first began to produce tornadoes. As this packet advanced rapidly across Ohio it carried a line of cells with it, apparent at 2335 GMT, with many destructive tornadoes. To the south it interacted weakly with the remains of area α producing few signs of rejuvenation of either party.

TABLE 3. Times (GMT) of tornadoes 3–4 April 1974, from NOAA *Storm Data*, for each convective area.

Area α	Area β			Area γ	
1905	1915	2210	0038	1907	0015 (2)
2030	1925	2212	0050	1912	0025
2100 (2)	1940	2218 (2)	0100	1938	0045 (3)
2115	1945	2230	0105	1945	0100
2130	2000	2252	0108	1951	0140
2200 (2)	2020	2300 (2)	0120 (2)	2010	0156
2221	2030	2302	0125	2025	
2235	2035	2310	0135	2048	
2250	2040	2315	0150 (2)	2055	
2330	2042	2330	0200	2125	
2332	2050	2335	0205	2130	
2345 (2)	2100	2347	0210	2150	
0000	2108	2348	0215	2250	
0100	2115	2358	0234	2330	
0105	2128	0000 (2)	0300	2335	
0115	2144	0005	0338	2345	
0200	2146	0022	0345	2350	
0235	2158	0030 (3)	0430 (3)	2355	
0245	2200 (3)	0032		0010	

Packet H, like D, appeared in eastern Iowa, but unlike D, to the accompaniment of thunderstorms which moved undestructively across northern Illinois. Between 2335 and 0235 GMT it overtook convective area γ, which began to produce numerous tornadoes after having been relatively quiescent since 2200 GMT. It also developed a substantial extension to the south, where it was a benign wake depression following packet D.

Packet I was short of both length and life. It formed among ill-organized cells near the northeastern edge of area β at 2335 GMT. It moved rapidly eastward producing large pressure fluctuations in northern Ohio but little severe weather except a single tornado in southeastern Michigan.

Packet J formed in a region of chaotic convection but widespread rain at the western edge of area α around 2335 GMT. It produced little organization in the cell structure, but there was a resurgence of tornado activity in the area after 2330 GMT (cf. Table 3), perhaps attributable to this packet.

In summary, the origin of packets A and B cannot be specified. Packets C, F and part of H formed as wake depressions to the rear of active convective systems; E and G formed simultaneously with vigorous convective lines; and I and J formed within ill organized regions of preexisting convection. Only with packet D was there no clear relationship to concurrent or prior convection. There was thus little indication of the initiation of convection by preexisting gravity waves, as described by Uccellini (1975).

Our results, however, agree with Uccellini's (1975) in that the clearest interaction was the reorganiza-

FIG. 10. Superposition of analyzed packet troughs, convective areas and cells and lines from radar summary maps, for indicated GMT times.

tion of cells in a convective region and the initiation or enhancement of the associated tornado activity which accompanied the overtaking of the slow-moving area by the fast-moving wavepacket. An increase in the pressure amplitude of the packet also characterized the overtaking. This occurred as D overtook γ, E overtook β, F overtook α, H overtook γ and perhaps as J overtook α. The persistence and continuity of wave packets as they passed through the convective regions was surprising.

9. Concluding questions

1) What is the mechanism of the development of discrete convective areas, oriented parallel to the low-level flow and ~150 n mi apart, during the late morning of 3 April? Vertical cross sections from southwest to northeast through the upwind edge of the convective region appear in Fig. 11. It appears that the convection occurred above a fraction layer with intense vertical shear, extending from the ground to ~1 km. Bulk Richardson numbers were around unity in this layer near PIA and SLO at 1200 GMT despite strong static stability. A single sounding was available at 1800 GMT, at BNA, showing an approximately adiabatic temperature structure and an only slightly diminished shear. Presumably, Richardson numbers fell below 0.25 fairly early in the period of morning heating, so that growing per-

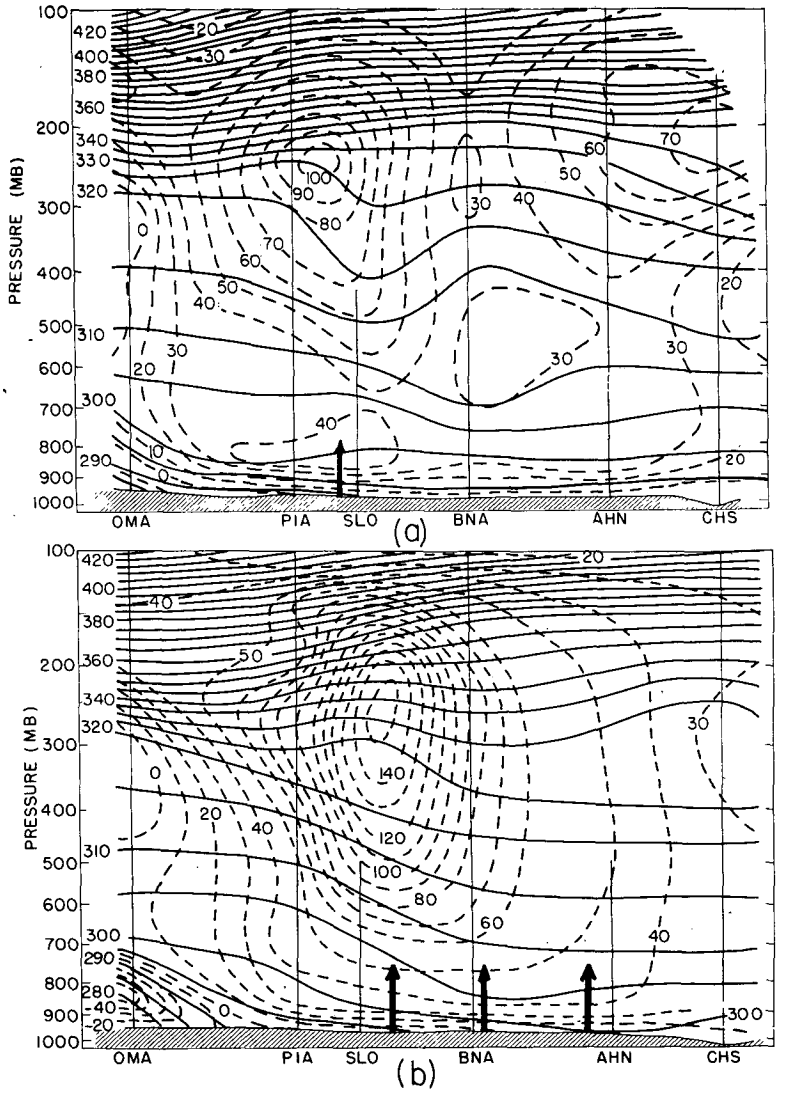

FIG. 11. Vertical cross sections of potential temperature at intervals of 5 K (solid) and of wind component into the section at intervals of 10 kt (dashed) for 1200 GMT 3 April (a) and for 0000 GMT 4 April (b). Locations of stations are shown in Fig. 3. Thin vertical lines show the extent of the wind soundings. Geostrophic estimates supplemented the observed wind data near the jet core. Approximate positions of the main convective regions are shown by heavy arrows directed upward from the ground.

turbations could have triggered the observed convection before adiabatic conditions were established throughout the subcloud layer. The spacing of the major convective regions, however, seems too large (250–300 km) to be attributable to perturbations growing in a layer only 1 km deep.

Further examination of the cross sections shows that the convection occurred in a region of anticyclonic shear through much of the troposphere, and was bounded on the northwest by the major jet core. Much of the depth of the convective layer was characterized by low absolute vorticity (probably negative in some regions) on surfaces of either constant pressure or constant potential temperature.

Parallel or inertial instability of some type, as proposed by Raymond (1978) and Emanuel (1979), may be responsible, but to the extent that they can be tested at all, the theories have not yet been developed to the point of yielding more than the roughest qualitative agreement.

2) Why was it possible for convective lines to advance as rapidly as their associated wavepackets at some times and places, but not generally?

3) Is it possible that the presumed gravity wavepackets also contained vorticity which provided the background against which development of rotating thunderstorms and tornadoes was encouraged?

Only a further development of theory and an enhanced vertical sounding capability can provide the answers. A special field program like SESAME '79 could be extremely fruitful, but the widespread provision of 1800 GMT soundings at regular National Weather Service stations on threatening days would be most helpful.

Acknowledgments. The authors are grateful to Professor Lance F. Bosart and to other members of the MIT Convection Club for comparative analysis and for useful discussion, and to the National Science Foundation, Atmospheric Sciences Division, for support under Grant ATM 74-24405 A01.

REFERENCES

Darkow, G. L., and R. L. Livingston, 1975: The evolution of the surface static energy fields on 3 April 1974. *Preprints Ninth Conf. Severe Local Storms*, Norman, Amer. Meteor. Soc., 264–269.

Emanuel, K. A., 1979: Inertial stability and mesoscale convective systems. Part I: Linear theory of inertial instability in rotating viscous fluids. *J. Atmos. Sci.*, **36,** 2425–2449.

Forbes, G. S., 1975: Relationship between tornadoes and hook echoes on 3 April 1974. *Preprints Ninth Conf. Severe Local Storms*, Norman, Amer. Meteor. Soc., 280–285.

Fujita, T. T., 1975: Super outbreak tornadoes of 3–4 April 1974. Map printed by University of Chicago Press. [Available from T. T. Fujita, Dept. of Geophysical Sciences, University of Chicago]

Galway, J. G., 1956: The lifted index as a predictor of latent instability. *Bull. Amer. Meteor. Soc.*, **37,** 528–529.

Hoxit, L. R., and C. F. Chappell, 1975a: Tornado outbreak of 3–4 April 1974: Synoptic analysis. NOAA TR ERL 338-APCL 37 [NTIS PB247361/AS].

——, C. F. Chappell and J. M. Fritsch, 1976: Formations at mesolows or pressure troughs in advance of cumulonimbus clouds. *Mon. Wea. Rev.*, **104,** 1419–1428.

Lindzen, R. S., 1974: Wave-CISK in the tropics. *J. Atmos. Sci.*, **31,** 156–179.

——, and K. K. Tung, 1976: Banded convective activity and ducted gravity waves. *Mon. Wea. Rev.*, **104,** 1602–1617.

Raymond, D. J., 1975: A model for predicting the movement of continuously propagating convective storms. *J. Atmos. Sci.*, **32,** 1308–1313.

——, 1978: Instability of the low-level jet and severe storm formation. *J. Atmos. Sci.*, **35,** 227–2280.

Uccellini, L. W., 1975: A case study of apparent gravity wave initiation of severe convective storms. *Mon. Wea. Rev.*, **103,** 497–513.